How Well Can We Represent the Spectrum of Convective Clouds in a Climate Model? Comparisons between Internal Parameterization Variables and Radar Observations

LAURENT LABBOUZ,[a] ZAK KIPLING,[b] AND PHILIP STIER

Department of Physics, University of Oxford, Oxford, United Kingdom

ALAIN PROTAT

Bureau of Meteorology, Melbourne, Victoria, Australia

(Manuscript received 23 June 2017, in final form 18 January 2018)

ABSTRACT

Current climate models cannot resolve individual convective clouds, and hence parameterizations are needed. The primary goal of convective parameterization is to represent the bulk impact of convection on the gridbox-scale variables. Spectral convective parameterizations also aim to represent the key features of the subgrid-scale convective cloud field such as cloud-top-height distribution and in-cloud vertical velocities in addition to precipitation rates. Ground-based radar retrievals of these quantities have been made available at Darwin, Australia, permitting direct comparisons of internal parameterization variables and providing new observational references for further model development.

A spectral convective parameterization [the convective cloud field model (CCFM)] is discussed, and its internal equation of motion is improved. Results from the ECHAM–HAM model in single-column mode using the CCFM and the bulk mass flux Tiedtke–Nordeng scheme are compared with the radar retrievals at Darwin. The CCFM is found to outperform the Tiedtke–Nordeng scheme for cloud-top-height and precipitation-rate distributions. Radar observations are further used to propose a modified CCFM configuration with an aerodynamic drag and reduced entrainment parameter, further improving both the convective cloud-top-height distribution (important for large-scale impact of convection) and the in-cloud vertical velocities (important for aerosol activation).

This study provides a new development in the CCFM, improving the representation of convective cloud spectrum characteristics observed in Darwin. This is a step toward an improved representation of convection and ultimately of aerosol effects on convection. It also shows how long-term radar observations of convective cloud properties can help constrain parameters of convective parameterization schemes.

1. Introduction

A large variety of convective clouds exist in the atmosphere, from liquid-phase-only shallow cumulus to deep convection, from single cells to organized systems. They play an important role in the climate system by redistributing energy, water, and tracers vertically and horizontally through their impact on the large-scale dynamics and their radiative effect. Convective clouds can produce large amounts of precipitation and hence have a significant impact on the hydrological cycle. The size of an individual convective cloud ranges from about 100 m up to several tens of kilometers and hence cannot be explicitly resolved by current climate models. Standard commonly used bulk mass flux schemes (e.g., Tiedtke 1989; Bechtold et al. 2001; Kim and Kang 2012)

Denotes content that is immediately available upon publication as open access.

Supplemental information related to this paper is available at the Journals Online website: https://doi.org/10.1175/JAS-D-17-0191.s1.

[a] Current affiliation: Laboratoire d'Aérologie, Université Paul Sabatier, Toulouse, France.

[b] Current affiliation: ECMWF, Reading, United Kingdom.

Corresponding author: Laurent Labbouz, l.labbouz@gmail.com

DOI: 10.1175/JAS-D-17-0191.1

do not explicitly represent the spectrum of convective clouds but aim to represent its bulk effect on the large scale through gridbox-mean mass fluxes with height-dependent entrainment and detrainment rates. Hence, as they do not explicitly calculate in-cloud vertical velocities, they suffer from strong limitations in the treatment of microphysical processes (Sullivan et al. 2016) and aerosol–cloud interactions, possibly leading to deficiency in their ability to estimate climate forcing (Donner et al. 2016). Contrary to bulk mass flux schemes, spectral convective parameterizations aim to represent a population of convective clouds in a deterministic (e.g., Arakawa and Schubert 1974; Moorthi and Suarez 1992; Wagner and Graf 2010; Yoshimura et al. 2015) or stochastic way (e.g., Plant and Craig 2008).

The convective cloud field model (CCFM; Nober and Graf 2005; Wagner and Graf 2010; Kipling et al. 2017) is a spectral convective parameterization based on the Arakawa and Schubert (1974) concept of quasi equilibrium of a population of convective clouds with the large-scale forcing. It has been implemented in the aerosol–climate model ECHAM6.1–HAM2.2 (Kipling et al. 2017), which is the sixth version of ECHAM, the Max Planck Institute for Meteorology atmospheric general circulation model, (Stevens et al. 2013) coupled with the aerosol model HAM (Stier et al. 2005; Zhang et al. 2012). Kipling et al. (2017) improved CCFM by adding a subcloud parcel model to trigger convection and calculate cloud-base vertical velocity in order to achieve a physically based representation of cloud properties and a better link with the boundary layer temperature and humidity profiles. Global simulations using this version of CCFM in ECHAM6.1–HAM 2.2 have been evaluated against observations and performed better than the standard bulk mass flux Tiedtke–Nordeng scheme in representing the spatial distribution of precipitation and, in particular, the diurnal cycle of convection (Kipling et al. 2017). We will use ECHAM6.1–HAM2.2 in this study, hereinafter referred to as ECHAM–HAM.

To our knowledge, neither CCFM nor other spectral convective parameterizations have been compared with long series of observations of internal parameterization variables (e.g., vertical velocity and mass flux). Studying internal parameterization variables rather than only the bulk impact of convection on the large scale is an important step toward better understanding the strengths and limitations of current parameterizations: this is the focus of the present study. More precisely, internal characteristics of the population of clouds modeled with the ECHAM–HAM single-column model (SCM) are compared to recent radar retrievals at Darwin, Australia (Kumar et al. 2015). The choice of Darwin for this study is driven primarily by the data availability, offering a unique opportunity to compare CCFM internal variables with long-term observations but also by the importance of tropical convection in the climate system.

SCM simulations are well constrained by the large-scale-forcing dataset driving them and hence provide a good framework for testing and developing parameterizations (Randall et al. 1996; Zhang et al. 2016). SCMs have been widely used for various model testing and for intercomparison studies (Ghan et al. 2000; Franklin et al. 2012; Neggers et al. 2012; Song et al. 2013; Zhang et al. 2013; Petch et al. 2014), made easier by the lack of large-scale dynamical feedback, although this is also one of the limitations of SCMs (Zhang et al. 2016).

We define the key characteristics of the cloud spectrum as (i) the distribution of cloud-top height as it controls detrainment height and hence strongly influences the radiative impact of convection and (ii) the in-cloud vertical velocity as it has a strong impact on supersaturation, aerosol–cloud interactions (activation), and microphysics. We will also discuss the spatial and temporal distributions of convective precipitation rates (which has societal and environmental impacts). Studying the sensitivity of these key convective cloud characteristics to model parameters and evaluating them against observations is a prerequisite for further use of CCFM to address the associated scientific questions (radiative impact, microphysics and aerosol–convection interactions, spatial and temporal heterogeneity of precipitation).

Rather than performing a fine-tuning experiment, we aim to understand how CCFM internal parameters (entrainment, drag, and triggering parameters) impact model results in terms of spectrum characteristics. We then compare CCFM results with the Tiedtke–Nordeng bulk mass flux scheme and with the radar retrievals in order to determine to what extent CCFM can simulate the observed convective cloud-top-height distribution and profiles of vertical velocity with a given set of parameters. In other words, what is needed in order for CCFM to simulate the observed convective cloud spectrum in the tropical western Pacific? Addressing this question will also provide an illustration of the usefulness of new radar retrievals for evaluating and developing convective parameterizations.

Section 2 presents the model configuration and new CCFM development performed for the current study. Section 3 gives a short overview of the Darwin radar data and the retrieval methods used. The SCM results are presented and compared with the radar retrievals in section 4. Conclusions and additional discussion are provided in section 5.

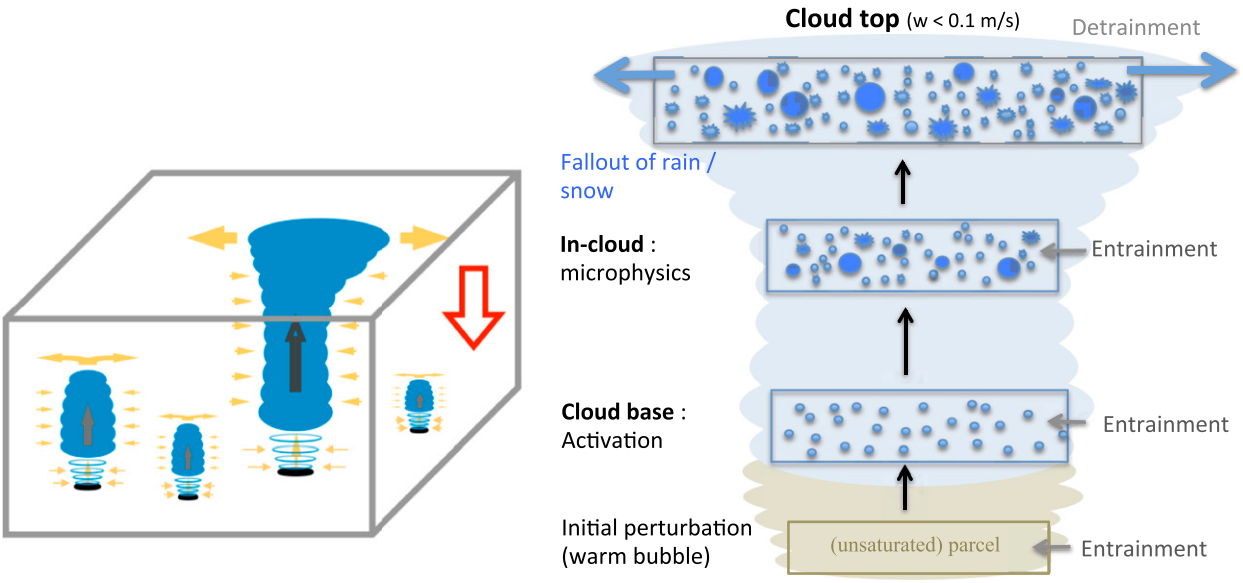

FIG. 1. (left) Schematic representation of the cloud field represented by CCFM (from Kipling et al. 2017); the red arrow represents the compensating subsidence that occurs in the GCM column. (right) Schematic of the Lagrangian entraining plume model used for each cloud type.

2. Model description

a. Convective parameterization

In this section, we provide a description of the main features of CCFM relevant for this study and highlight the differences to previous studies using CCFM (Wagner and Graf 2010; Kipling et al. 2017).

Our main focus is on CCFM, but we also use the Tiedtke–Nordeng bulk mass flux scheme (Tiedtke 1989; Nordeng 1994) for comparisons. The main features of the Tiedtke–Nordeng scheme relevant for this study are the differences with CCFM: it represents only one average convective cloud that can be shallow, midlevel, or deep, and it has a simple model for entraining downdrafts (each updraft type and the downdrafts have their own prescribed fractional entrainment rate). The bulk mass flux calculation does not involve any explicit calculation of vertical velocity or convective area, contrary to CCFM, which gives vertical velocity and cloud radius and calculates the mass flux from them (cf. hereafter and supplemental section S1). More details can be found in Tiedtke (1989) and Nordeng (1994) as well as in Möbis and Stevens (2012) and Stevens et al. (2013) for the implementation in ECHAM6.

1) CCFM GENERAL CONCEPT

The CCFM (Fig. 1) is based on the idea of convective quasi equilibrium (Arakawa and Schubert 1974): the slowly varying large-scale processes destabilize the atmosphere, and the comparatively fast convective response leads to an "equilibrium" between large-scale forcing and convection. In other words, at every model time step, the convective parameterization tends to remove the large-scale-generated convective available potential energy (CAPE). The CAPE is consumed not by a single average cloud but by a population of clouds of different radii. Within a given model column, CCFM represents a spectrum of up to 10 cloud types. Each cloud type is defined by its cloud-base radius, and there may be several clouds of a given type within one column of the host model ECHAM–HAM. CCFM is hence designed to (simultaneously) represent both shallow and deep convection.

The new triggering scheme introduced by Kipling et al. (2017) aims to represent the impact of the subcloud layer (convective inhibition) on convective initiation and cloud-base properties such as vertical velocity (Fig. 1). Entraining plumes of radii ranging from 100 m to the depth of the boundary layer are initiated by perturbing the temperature (adding T_{init} to the resolved-scale temperature) and specific humidity (adding q_{init}) at L_{init} model levels above the lowest vertical level. Kipling et al. (2017) used a quite large temperature perturbation $T_{\text{init}} = 2.8\,\text{K}$ and a small humidity perturbation $q_{\text{init}} = 0.1\,\text{g}\,\text{kg}^{-1}$ starting from the model level $L_{\text{init}} = 2$ to obtain optimal results overall in global simulations (and top-of-the-atmosphere radiative balance) but not specifically in the Tropical Warm Pool–International Cloud Experiment (TWP-ICE) domain. The TWP-ICE domain is located in a mostly tropical maritime

environment with moderate temperature spatial variability and a rather flat terrain with only small hills inland (May et al. 2008, their Fig. 1) so that temperature perturbations are likely to be moderate and to occur at low altitude. Hence, the standard values in this study are $L_{\text{init}} = 1$ (first level above the model level containing the surface, corresponding to an altitude of about 155 m), $T_{\text{init}} = 1$ K, and $q_{\text{init}} = 0.1\ \text{g kg}^{-1}$. The model parameters T_{init}, q_{init}, and L_{init} can be adjusted: the differences with the Kipling et al. (2017) configuration are analyzed in sections 4a and 4b(1), while for brevity, the sensitivity to T_{init}, q_{init}, and L_{init} is discussed in more detail in the supplement (see section S2 and Figs. S1–S5).

Depending on temperature and specific humidity profiles, some of the plumes may rise up to their levels of condensation and form a cloud. The smallest and the largest plumes reaching their condensation levels set the minimum and maximum cloud-base radius and the CCFM cloud model is run for 10 "clouds" (each of them is represented by a rising plume) of cloud-base radius linearly increasing between these boundaries. For each CCFM cloud, all the phase changes and the precipitation formation are calculated until the cloud reaches its cloud top, defined as the altitude where the vertical velocity is smaller than $0.1\ \text{m s}^{-1}$ (Fig. 1).

At cloud base, the cloud droplet number concentration (CDNC) is obtained by activating the available cloud condensation nuclei (Abdul-Razzak and Ghan 2000). The microphysics calculations within each plume are based on Zhang et al. (2005). The vertically varying variables within the plume model (i.e., "prognostic" variables in a Lagrangian sense and within one host model time step) are the vertical velocity, plume radius, temperature, and bulk mixing ratios of cloud liquid, cloud ice, rain, and snow [as in Wagner and (Graf 2010) and Kipling et al. (2017)]. For this study, the microphysics is still based on Zhang et al. (2005), but contrary to previous CCFM studies, CDNC can also vary vertically within one plume: effects of dilution due to entrainment, autoconversion, and accretion on CDNC are now taken into account (and are sinks for CDNC), while in previous versions, these processes were only changing mass concentrations. Droplet activation is unchanged and occurs only at cloud base. All hydrometeors are detrained at cloud top and are a source for the large-scale (stratiform) cloud scheme, which includes fully prognostic CDNC and liquid and ice mixing ratios at the ECHAM–HAM grid scale (Lohmann et al. 2007; Lohmann and Hoose 2009).

The calculation of the cloud spectrum (i.e., the number of clouds of each type) is obtained by solving a Lokta–Volterra system of equations, representing the competition of the different cloud types (predators) for the available energy (prey). The details of the theoretical derivation are given by Wagner and Graf (2010), while some more information about the current version of CCFM in the aerosol–climate model ECHAM6.1–HAM2.2 as well as its evaluation can be found in Kipling et al. (2017).

2) CCFM PLUMES' EQUATION OF MOTION

The forces acting on the rising parcel are the thermal buoyancy, the gravitational force acting on suspended hydrometeors (weight of hydrometeors lifted), and the aerodynamic drag. An additional term may be added to account for inertial effects.

This "inertial" term exists in any flow (including non-viscous irrotational ones) and is proportional to the total acceleration of the parcel (Brennen 1982). It is sometimes referred to as "added drag" and accounts for the fact that when the parcel rises it has to move the surrounding air (the environment), and this leads to an increased effective inertia. It is usually written as a virtual (or added) mass (Saunders 1962; Turner 1963; Brennen 1982; Pantaleone and Messer 2011). We will only use this formulation and refer to it as *virtual mass*. The aerodynamic drag does not depend on the acceleration but on the velocity of the parcel; we refer to it simply as *drag*.

The equation of motion of a rising parcel can then be written as (Simpson et al. 1965; Simpson and Wiggert 1969)

$$\frac{dw}{dz} = \frac{1}{w}\frac{dw}{dt} = \frac{1}{1+\gamma}\left(g\frac{T_{v_{\text{cloud}}} - T_{v_{\text{env}}}}{T_{v_{\text{env}}}} - g\frac{q_c}{w} - \frac{C_\mu}{2r}w - \frac{3}{8}\frac{C_d}{r}w\right), \tag{1}$$

where w is the in-cloud vertical velocity ($w > 0$), $\gamma = 0.5$ the virtual mass coefficient [Turner 1963; Pruppacher and Klett 1997, chapter 12, Eqs. (12)–(25); Pantaleone and Messer 2011], g the gravitational acceleration, $T_{v_{\text{cloud}}}$ and $T_{v_{\text{env}}}$ the virtual temperatures for the cloud air and the environment, respectively, q_c the total mass mixing ratio of lifted water condensate, r the radius of the rising parcel, C_μ the entrainment parameter, and C_d the drag parameter. For completeness, the equation governing the cloud radius is included in the supplement (section S1). Apart from its direct effect on vertical velocity shown in Eq. (1) (entrainment of momentum), entrainment has a significant impact on buoyancy: entraining drier environmental air leads to evaporation or sublimation of hydrometeors, reducing the cloud virtual temperature and hence the cloud buoyancy (while drag does not have any impact on thermal buoyancy; cf. also section 4b).

TABLE 1. List of the simulations analyzed in the paper (excluding supplemental material). As described in the text, C_μ is the entrainment-rate parameter, T_{init} the initial temperature of the parcel, C_d the drag parameter, and L_{init} the height level of the initial perturbation (counted from the surface: 0 is the surface level). All CCFM simulations use an initial humidity perturbation $q_{\text{init}} = 0.1\ \text{g kg}^{-1}$. The last column indicates whether the new equation of motion or the former one is used. Additional simulations varying the virtual mass gamma as well as q_{init}, T_{init}, and L_{init} are presented as supplemental material (section S2 and Figs. S1–S6). Choices for parameters values are explained in the text.

	C_μ	T_{init} (K)	C_d	L_{init} (level above surface)	New equation of motion [Eq. (1)]
CCFM_K2017	0.2	2.8	0	2	No [Eq. (2)]
Cmu0.2_2.8K_l2	0.2	2.8	0	2	Yes
Cmu$Y$	Y = 0.2, 0.07, 0.03, 0.01	1.0	0	1	Yes
Cmu0.03_CdZ (low entrainment)	0.03	1.0	Z = 0, 0.6, 1, 1.5	1	Yes
Tiedtke–Nordeng scheme					
Tiedtke–Nordeng [default for ECHAM–HAM; as in Kipling et al. (2017)]					
Tiedtke–Nordeng entrainment rate/10 (all entrainment rates divided by 10)					

The original equation of motion in Simpson and Wiggert (1969) is as follows:

$$\frac{dw}{dz} = \frac{1}{1+\gamma} g \frac{T_{v_{\text{cloud}}} - T_{v_{\text{env}}}}{T_{v_{\text{env}}}} - g\frac{q_c}{w} - \frac{C_\mu}{2r} w - \frac{3}{8}\frac{C_d}{r} w\,, \quad (2)$$

which assumes implicitly that the virtual mass effect applies only on buoyancy. We believe this is an unnecessary approximation of the concept of virtual mass [which is an inertial effect and should hence modify the *total* acceleration; cf., e.g., Pantaleone and Messer (2011) for a general discussion and also Pruppacher and Klett (1997, chapter 12)]. Earlier versions of CCFM (Wagner and Graf 2010; Kipling et al. 2017) as well as other convective parameterizations (Gregory 2001; Guérémy 2011) are based on this original Simpson and Wiggert (1969) formulation. In this study, we adopt the corrected equation (Table 1) except for CCFM_K2017 simulations. It is important to note that there are only small fundamental differences between the corrected equation and the older one: most of the changes can be offset by changing the value of the tunable parameters C_μ and C_d (scrutiny of the equation shows that the only difference lies in the gravity of the hydrometeors, which has a lower relative impact in the new formulation than in the original one).

The entrainment term (Levine 1959; Simpson and Wiggert 1969) relies on the assumption of continuous and homogeneous mixing. It is a widely used simple representation of the complex turbulent processes leading to the entrainment of environmental air into the cloud (Arakawa and Schubert 1974; Kain and Fritsch 1990). Large-eddy simulations suggest limitations of this approach for representing shallow convection (Dawe and Austin 2013) and possibly the need for different parameter values depending on updraft type (Wang and Zhang 2014). However, in the framework of our rather simple entraining plume model, we keep a single, constant value of C_μ for all clouds and all conditions. Note that although the entrainment parameter C_μ is constant, the fractional entrainment rate is given by C_μ/r (Wagner and Graf 2010) and hence is inversely proportional to the cloud radius (cf. also section S1).

The drag term follows the classical formulation, neglecting the small density difference between the parcel and the environment (cf., e.g., Levine 1959). The drag parameter C_d is not very well constrained, as it depends on the flow characteristics (Reynolds number and shape of the plume) and on assumptions on the turbulence (Simpson et al. 1965). Simpson et al. (1965) propose $C_d = 0.506$ (widely used in the literature since then) for a given entrainment rate but warn that similar results could be obtained with other values of C_d and that they cannot conclude on its magnitude. They also highlight that the virtual mass and drag coefficients, although different, have similar effects on the plume development (by reducing its acceleration). Based on these conclusions, latter models have used various empirical configurations.

The set of values used from C_d and γ varies from model to model. Simpson and Wiggert (1969) compare simple cumulus model simulations using $C_d = 0.506$ and $\gamma = 0$ and $C_d = 0$ and $\gamma = 0.5$ and argue that the latter has better support from laboratory experiment and some observations (but limited and rather qualitative). Previous formulations of CCFM (Wagner and Graf 2010; Kipling et al. 2017) adopted this configuration ($C_d = 0$, $\gamma = 0.5$). Bretherton et al. (2004) give a different definition of the coefficients and use a formulation with only a drag coefficient and setting the virtual mass coefficient γ to zero. Several bulk mass flux parameterizations adopt $\gamma = 0.5$ and a nonzero value of the

drag coefficient (Gregory 2001; Guérémy 2011) based on Simpson et al. (1965). Sherwood et al. (2013) model thermals as Hill's vortices and argue that the passive drag can then be neglected but discuss the possibly important turbulent dissipation and virtual mass (i.e., inertial) effects. In contrast, Romps and Charn (2015) show that in their simulations tropical maritime thermals differ from Hill's vortices and drag plays an important role, while the virtual mass effect can be neglected as the actual net acceleration of plumes is small.

In our study, we keep the standard, widely used value of $\gamma = 0.5$ and only briefly discuss the impact of changing γ compared to changing C_d. We investigate the impact of different values of the poorly constrained and somehow controversial drag coefficient C_d: 0 for a no-drag simulation; 0.6, as in Romps and Charn (2015); 1, which is close to the value for a sphere; and a stronger drag of 1.5. We also discuss the impact of the other poorly constrained parameter, the entrainment parameter C_μ. The different configurations are compared with radar observations of convective clouds, as well as with the original configuration of CCFM (from Kipling et al. 2017) and the Tiedtke–Nordeng scheme. A list of simulations is provided Table 1.

b. Model configuration

We use CCFM in the ECHAM6.1–HAM2.2 SCM. The SCM has the same physics as the full ECHAM–HAM, but the model dynamics is replaced by prescribed horizontal advective tendencies of specific humidity and temperature. The large-scale vertical and horizontal winds as well as the surface pressure and the surface temperature are prescribed at every time step (the surface moisture and energy fluxes are not).

The 6-hourly data used to drive the SCM are provided by the Department of Energy Atmospheric Radiation Measurement (ARM; Xie et al. 2010) Program. They are based on a variational analysis using ECMWF operational analysis in the four grid points encompassing the domain of the TWP-ICE (May et al. 2008), in Darwin, Australia. Additionally, microwave radiometer measurements of liquid water path and radar-derived precipitation rates are used to constrain the variational analysis (Zhang and Lin 1997; Xie et al. 2004). The forcing dataset is currently available for three wet seasons (November–April), but we focus only on the wet seasons 2005/06 and 2006/07 (cf. section 4 and supplemental material) during which radar data were also available.

We use the standard vertical resolution for ECHAM6.1–HAM2.2: 31 vertical levels and a 12-min time step. Convection is parameterized with either CCFM or the default bulk mass flux Tiedtke–Nordeng scheme (Tiedtke 1989; Nordeng 1994; Stevens et al. 2013).

The lack of feedback in SCM simulations can lead to a significant drift in temperature and humidity through model errors associated with the lack of large-scale feedback and from errors in the forcing data, accumulating over the course of the simulation (Zhang et al. 2016). To avoid this problem, one approach is to perform short successive simulations; another is to apply nudging (e.g., Neggers et al. 2012). We use the latter, as this gives similar benefits as having successive short simulations without the limitations related to reinitializing the model (and hence having discontinuous time series). The model is relaxed to the vertical profiles of specific humidity and temperature following the equation

$$x = x^0 + (x^f - x^0)\frac{\Delta t}{\tau}, \tag{3}$$

where x is the variable (specific humidity or temperature) value after relaxation has been applied, x^0 its value before relaxation, x^f the target value to relax to, $\Delta t =$ 12 min the model time step, and $\tau = 6$ h the relaxation time scale. We choose this relaxation time of 6 h, as it is the time resolution of the variational analysis data. It is also long enough to provide the model with some level of freedom without allowing for any significant drift (Neggers et al. 2012).

3. Radar data

The radar products used in this study are described in Kumar et al. (2015). We provide here a brief overview of the most important features for the present study, as well as some details about specific choices we make.

Vertically pointing ultra-high-frequency (UHF) and very-high-frequency (VHF) radars at, respectively, 920 and 50 MHz are used for high-accuracy retrievals of in-cloud vertical velocity at Darwin (Williams 2012). The use of two frequencies is needed to separate the air vertical velocity from the velocity of the falling hydrometeors (Protat and Williams 2011). Profiler retrievals are provided every minute with 100-m vertical resolution from 1.7 to 17 km, with the highest confidence below 11 km due to the limited sensitivity of the UHF profiler.

The C-band polarimetric radar (CPOL) provides volumetric data from plan position indicator (PPI) volumetric sampling and range–height indicator (RHI) scans over the site of the profilers. The radar reflectivity field is used to estimate surface precipitation rates on a 2.5-km horizontal grid every 10 min. CPOL RHI data are also used to classify the collocated UHF–VHF profiles as convective, mixed (or uncertain), or stratiform (Thurai et al. 2010). To consider all the convective profiles and to be as inclusive as possible, in this study, the "convective profiles" are those being flagged as

either mixed or (purely) convective at 2.5-km height. Including the mixed profiles does not significantly change the results compared to using only purely convective profiles: it only leads to a slight decrease in the average vertical velocity and in the relative occurrence of cloud tops at altitude above 15 km (not shown). CPOL resolution is 10 min, and hence, we assume that the pixel classification applies to interval $[t - 5\,\text{min}; t + 5\,\text{min}]$, meaning that if the CPOL profile at time t is convective, all the UHF–VHF 1-min profiles in the interval are considered as convective.

Statistics of cloud-top height are also derived from the CPOL profiles by estimating the 0-dBZ echo-top height (ETH). To account for shallow nonprecipitating convection, we do consider all the CPOL profiles with a valid reflectivity measurement at 2.5 km. We then weight every CPOL ETH by the number of profiles in the 10-min interval having at least one valid nonzero UHF–VHF retrieval of vertical velocity, and the probability distribution of cloud-top height is calculated using these weights. We use this unrestrictive criterion on vertical velocity, as more constraining ones (e.g., imposing to have at least one measurement of vertical velocity greater than $0\,\text{m s}^{-1}$ or even greater than $1\,\text{m s}^{-1}$) lead to very moderate changes in the probability distributions.

Following Kumar et al. (2015), we assume that the statistics of vertical velocity and cloud-top height at Darwin are representative of the TWP-ICE domain (cf. May et al. 2008, their Fig. 1). We also derive the convective mass flux similarly to Kumar et al. (2015), assuming that the fraction of CPOL profiles flagged as convective in a 9-h time window gives a good estimation of the mean convective area fraction in the model column (i.e., the TWP-ICE domain) and, more importantly for our study, that the mass flux can then be derived by assuming that every 1-min profile of vertical velocity flagged as convective shares an equal proportion of the convective area fraction. Kumar et al. (2015) showed that this method of using a ''time approach'' to estimate spatial area fraction gives relatively good results when compared to direct area fraction measurements, with however significant differences above about 8-km height where the method underestimates the area fraction and hence the mass flux (Kumar et al. 2015, their Fig. 2).

Apart from these methodological limitations in the calculation of the mass flux, there are also uncertainties associated with the radar retrievals. The horizontal resolution may limit the detection of intense localized precipitation, can affect the distribution of precipitation, and possibly lead to an underestimation of the occurrence of very heavy precipitation. As the profilers are close to the CPOL radar, echo-top-height calculations derived from CPOL should not be significantly affected by attenuation.

4. Results

This section contains three subsections. Section 4a provides an overview of the base simulations during the 2005/06 wet season (Tiedtke–Nordeng and base CCFM simulations) and a comparison with observations in terms of the key characteristics of the cloud spectrum (cloud-top height, vertical velocity, and mass flux). Section 4b discusses the sensitivity of these spectrum characteristics to model parameters (Table 1) and compares the broad performance of different configurations. Section 4c extends the analysis by focusing on selected model configurations to study the precipitation response.

a. *Base simulations*

As discussed in section 2b, theoretical considerations drive the use of a new equation of motion rather than the one used in earlier work with CCFM. For completeness, we provide comparisons between the configuration based on Kipling et al. (2017), CCFM_K2017, and an identical configuration but using the corrected equation of motion (Cmu0.2_2.8K_l2; cf. Table 1) as well as comparisons to the Tiedtke–Nordeng scheme and the radar retrievals (Fig. 2).

We observe (Fig. 2a) that during the 2005/06 wet season (10 November 2005–15 April 2006) the radar data exhibit two peaks in the distribution of cloud-top height (CTH), one around 6 km and another one around 13 km (recall that CTH cannot be retrieved below 2.5 km). The Tiedtke–Nordeng scheme produces sharp peaks at 1, 5, and 8 km, very different from the observations, and fails to produce any of the deepest convective clouds (above 10 km). The Tiedtke–Nordeng scheme allows for clouds of different heights but uses three prescribed cloud types with a prescribed fractional entrainment for each. The sharp peaks observed in the Tiedtke–Nordeng simulations are likely related to this discrete classification of convection types as either ''shallow,'' ''midlevel,'' or ''deep'' (Tiedtke 1989; Nordeng 1994). The two CCFM simulations produce smoother, more realistic CTH distributions. However, CCFM tends to overestimate the occurrence of cloud tops at about 3–4 and 6–10 km. The deepest clouds (CTH $>$ 12 km) are underrepresented, especially with CCFM_K2017. Cmu0.2_2.8K_l2 indeed produces deeper updrafts than CCFM_K2017 as applying the virtual mass to the total acceleration [Eq. (1)] rather than only to the buoyancy term [as in Eq. (2)] means that all terms reducing the acceleration (drag, condensate gravity, and

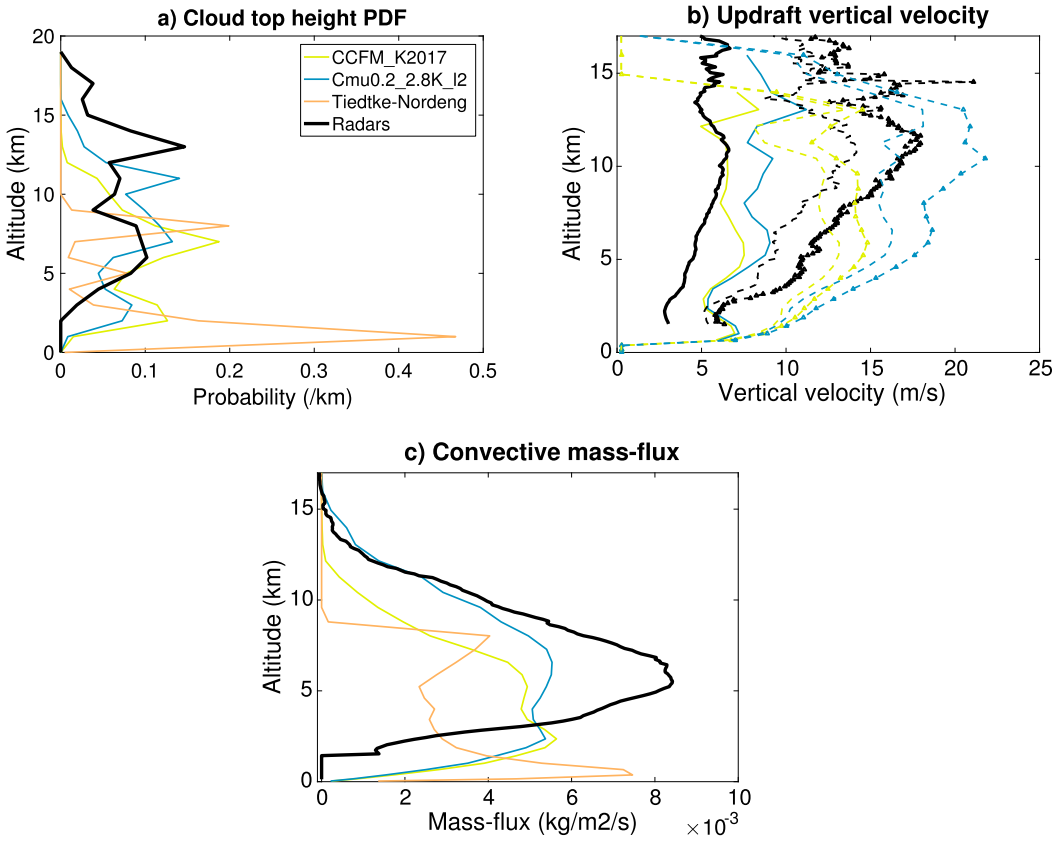

FIG. 2. Convective cloud spectrum characteristics from ECHAM6–HAM2 SCM simulations and radar retrievals at Darwin for the period from 10 Nov 2005 to 15 Apr 2006 (wet season). (a) Convective cloud-top-height distribution with 1-km vertical bins; (b) convective cloud updraft velocity (radar observations restricted to updrafts of 1 m s^{-1} and more) mean and 90th and 95th percentiles (solid lines, dashed lines, and dashed lines with triangles, respectively); and (c) convective mass flux. The plots are from radar retrievals (black lines), simulations with two different configurations of CCFM (yellow and blue lines; cf. Table 1 and text), and with the Tiedtke–Nordeng parameterization. Note that radar retrievals of vertical velocity and hence mass fluxes are available only between 1.7 and 17 km, with the highest confidence up to 11-km height [(b) and (c)], while cloud-top-height retrieval is available only above 2.5 km [(a)].

entrainment of momentum) are smaller in the new version than in the older one (everything else being kept unchanged).

The observed average vertical velocity (Fig. 2b) increases from about 3 to about 6.5 m s^{-1} at 11 km. The 90th and 95th percentiles profiles have a similar shape to the mean but stronger slopes. The simulations both have too-strong updrafts below 7 km (in term of mean and high percentiles). Above 7 km, the CCFM_K2017 simulation gives a mean vertical velocity close to the observations but 90th and 95th percentiles that are too small. Moreover, the simulated decrease of vertical velocity with height does not match the observations. Hence, both simulations have some difficulties in representing well the vertical velocity profile, and it is not obvious which one agrees better with the observations.

The radar-retrieved convective mass flux (Fig. 2c) has a maximum at 6 km and a small local maximum at 1.7 km, which could also give support to the idea of an unobserved mode of shallow clouds (however, more observations would be needed to confirm this hypothesis, and we hence exclude the shallowest clouds from our discussion). As mentioned in section 3, the radar-retrieved mass flux at 8 km and above is likely to be underestimated, possibly leading to an overestimation of the peak (relative) strength at 6 km. In comparisons with the radar retrievals, the Tiedtke–Nordeng mass flux profile has unrealistically sharp peaks (reflecting the peaks observed Fig. 2a), while the two CCFM simulations are in better agreement with the observations. They do not, however, reproduce the maximum of the mass flux at 6 km. The simulation with the corrected equation of motion (Cmu0.2_2.8K_l2) gives slightly better results than CCFM_K2017, the magnitude of the mass flux being closer to the radar retrievals at higher altitude.

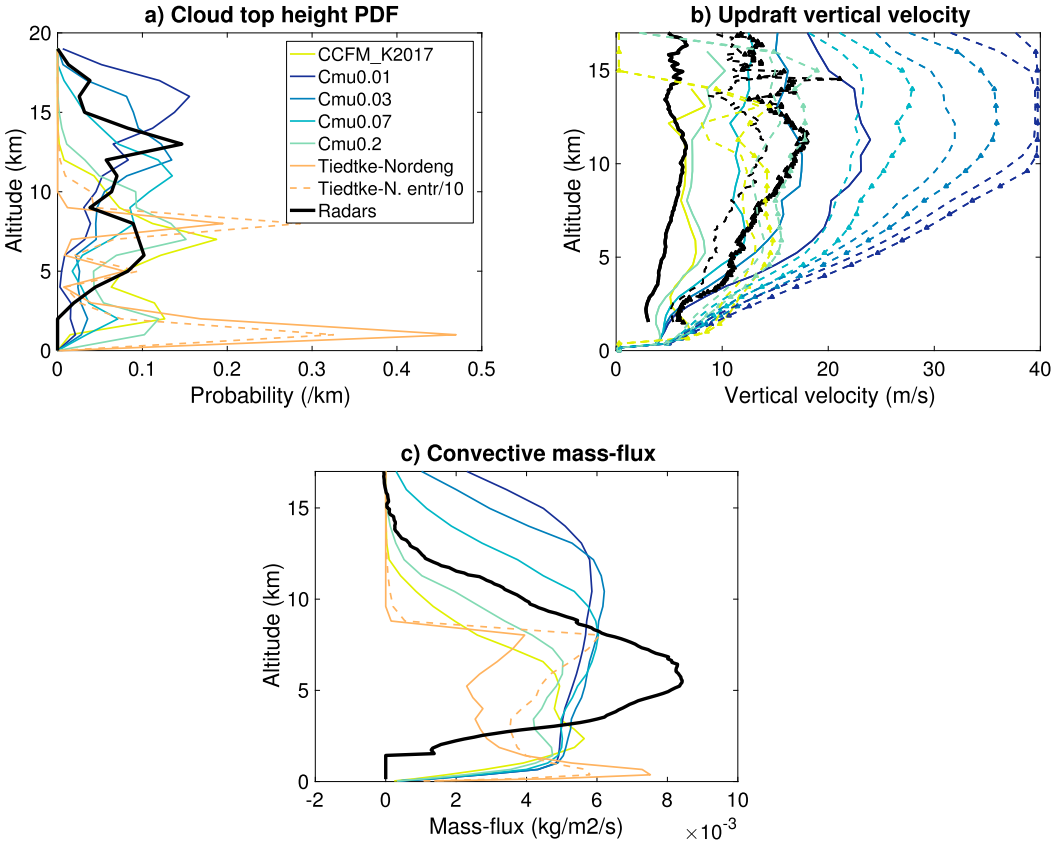

FIG. 3. As in Fig. 2, but for different values of the entrainment-rate parameter in CCFM. For comparisons, the (fixed) entrainment-rate parameters in Tiedtke have also been changed, and the dashed orange line is for a simulation with all the Tiedtke–Nordeng entrainment-rate parameters divided by 10. The triggering parameters are $L_{\text{init}} = 1$ and $T_{\text{init}} = 1$ K (cf. Table 1). Note that for output purposes the vertical velocities are put into bins, and the largest bin is 40 m s^{-1}, explaining the shape of the 90th and 95th vertical velocity percentiles for Cmu0.01.

Compared to CCFM_K2017, the simulation with the new equation (Cmu0.2_2.8K_l2) produces more deep clouds and a larger convective mass flux in better agreement with the radar products (Fig. 2). However, Cmu0.2_2.8K_l2 also has larger vertical velocities, especially above 4 km, showing reduced agreement with the observations. Hence, we cannot conclude which simulation gives the best results, and the sensitivity to parameters of CCFM_K2017 (not shown) is very similar to the one of the new version (discussed in section 4b): our motivation for using the corrected equation of motion remain driven by theoretical considerations.

b. *Cloud spectrum parameter sensitivity*

We study here the sensitivity of the convective cloud spectrum characteristics (cloud-top-height distribution, vertical velocity, and mass flux profiles) to CCFM parameters (entrainment and drag parameters; cf. Table 1) in order to understand how these parameters drive the spectrum and affect the comparison with observations.

Overall, changing the temperature, humidity, or height of the perturbation (cf. section S2 and Figs. S1–S5 for a discussion of the triggering parameters) does not lead to a significantly better agreement with the observations: improving the CTH distribution and the mass flux can only be achieved at the expense of the vertical velocity profile (and vice versa).

1) ENTRAINMENT

The entrainment-rate parameter C_μ is known to play an important role in the representation of shallow and deep convection. Reducing the entrainment-rate parameter increases the occurrence of higher clouds in both CCFM and Tiedtke–Nordeng (Fig. 3a). However, even with 10-times-smaller entrainment-rate parameters (compared to the default values), the Tiedtke–Nordeng scheme does not produce any cloud above 12 km and keeps the same unrealistically sharp peaks in the distribution at 1, 5, and 8 km (Fig. 3a). Decreasing the entrainment-rate parameter in CCFM leads to a

monotonic increase of the occurrence of deep convective clouds (high cloud tops). With an entrainment-rate parameter $C_\mu = 0.03$, CCFM is in reasonably good agreement with the observed distribution of convective cloud-top height (Fig. 3a) for cloud tops above 9 km, although the occurrence of cloud tops around 15 km is overestimated, and the occurrence of cloud tops around 6 km is largely underestimated.

This improvement in representing the cloud-top-height distribution by reducing the entrainment rate is obtained at the expense of far-too-strong updrafts (Fig. 3b). Indeed, reducing the entrainment rate reduces the evaporative cooling because of mixing with drier air; and reducing evaporation has a positive impact on buoyancy and hence increases the vertical velocity (reducing entrainment also reduces the slowing of the parcel because of entrainment of motionless air, but this is insignificant compared to the reduced evaporation effect).

Increasing the entrainment parameter increases the Tiedtke–Nordeng mass flux, which is then closer to the radar-derived values but still has a too-sharp peak and is much too small above 8 km (Fig. 3c). In CCFM, reducing the entrainment-rate parameter leads to an average mass flux closer to the observations in the midtroposphere (at 4–8 km, with $M_{\text{CCFM}} \sim 6 \times 10^{-3}\,\text{kg m}^{-2}\,\text{s}^{-1}$ and $M_{\text{radar}} \sim 6\text{–}9 \times 10^{-3}\,\text{kg m}^{-2}\,\text{s}^{-1}$; cf. Fig. 3c). The CCFM mass-flux profile is still too flat, while the observations show a maximum at 6 km (as discussed in section 4a). CCFM also overestimates the mass fluxes above 10 km for $C_\mu \leq 0.07$.

The shape of the radar-retrieved mass flux profiles seems quite robust: it does not change significantly if we use only the upward mass flux with vertical velocity above $1\,\text{m s}^{-1}$ in order to calculate the mean profile instead of considering all the profiles with at least one nonzero valid measurement (not shown). This is partly due to compensation between the negative downward mass flux and the small upward mass flux with $w < 1\,\text{m s}^{-1}$. As discussed in section 3, there are also limitations associated with the method used to retrieve mass fluxes. An accurate representation of the mass flux profile is difficult, and even idealized CRM simulations show differences, some models predicting mass flux profiles with a clear maximum in the midtroposphere while others have a flatter profile (Derbyshire et al. 2004, their Fig. 4), similar to the CCFM ones (Fig. 3c).

2) DRAG

Drag reduces the vertical velocity while keeping the buoyancy constant. In consequence, adding drag has a moderate effect on the cloud-top-height distribution and mass flux profiles, and this effect tends to saturate ($C_d = 0.6$, 1, and 1.5 give similar cloud-top heights and mass fluxes; cf. Figs. 4a and 4c). More precisely, the occurrence of very deep convective clouds (CTH > 13 km) is reduced and slightly underestimated in the simulations with drag (Cmu0.03_Cd0.6, Cmu0.03_Cd1, and Cmu0.03_Cd1.5), while the midtroposphere clouds are better represented than in Cmu0.03_Cd0 (Fig. 4a). The mass flux profile is slightly improved when drag is added (with a reduced overestimation above 10-km height; cf. Fig. 4c), although as discussed before, the profile remains too flat in the midtroposphere. The vertical velocity profile is largely improved: CCFM updrafts remain too strong but are in closer agreement with the observations for $C_d = 1.5$ (Cmu0.03_Cd1.5; cf. Fig. 4b) than in simulations without drag. Note that increasing the virtual mass coefficient γ has a similar effect to increasing the drag parameter C_d but with a smaller sensitivity (Fig. S6).

Further analysis shows that, although drag brings significant improvement, CCFM systematically tends to underestimate the occurrences of weak updrafts, which contribute largely to the observed convective cloud fraction (section S3 and Fig. S7). We believe this is related to intrinsic limitations of the plume model and its assumptions. CCFM performs similarly when used to simulate another wet season, confirming our results (section S4 and Fig. S8). CCFM simulations tend however to be less sensitive to changes in environmental conditions (especially humidity) than the observed convective cloud properties (sections S4 and S5; Figs. S8 and S9). Further investigation would need an additional long-term 3D dataset to perform more stratification of the data.

Hence, reducing the entrainment and adding drag (within the corrected equation of motion) allows for a better representation of both the CTH distribution (especially for the deeper clouds that were otherwise missing) and the vertical velocity profile, compared to the CCFM_K2017 simulations. This cannot be achieved by changing other parameters (triggering or entrainment alone). We do not aim here to provide any fine-tuning of CCFM, which has to be conducted in global simulations: we consider Cmu0.03_Cd1.5 as a satisfactory low entrainment–high drag configuration (cf. Fig. 5, which summarized the results on a few selected configurations).

c. *Extended analysis based on selected model configurations*

Section 4b discussed parameter sensitivities and showed that entrainment and drag parameters have significant impacts on CCFM vertical velocities and cloud-top-height distributions as well as on mass flux profiles. In this section, we expand our analysis to precipitation based on selected model configurations (Fig. 5).

The observed radar time series of precipitation during the 2005/06 wet season (10 November 2005–15 April

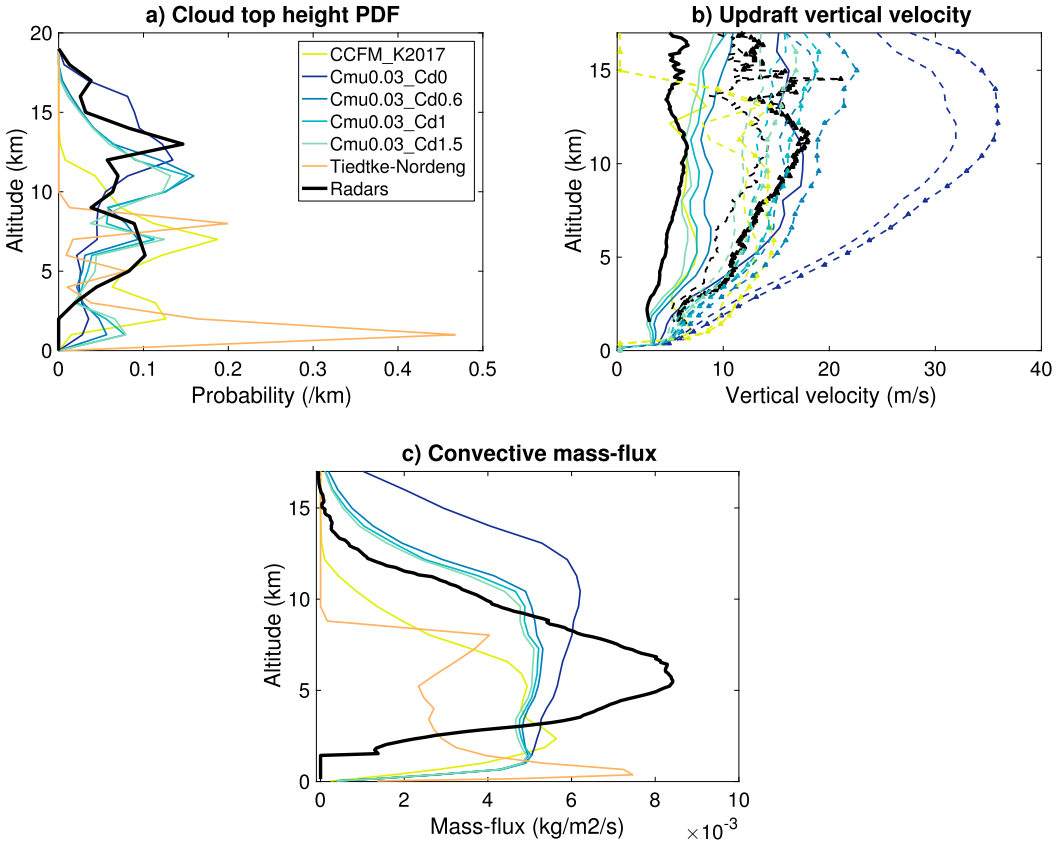

FIG. 4. As in Fig. 2, but for all the CCFM simulations made with $C_\mu = 0.03$ and with different values of the drag parameter (0, 0.6, 1, and 1.5 for colors from dark blue to light green).

2006) is well reproduced by CCFM (especially with a low entrainment parameter), while the bulk mass flux Tiedtke–Nordeng scheme tends to underestimate precipitation (Fig. 6a). The analysis of the 12-min SCM results (Fig. 6b) shows that Tiedtke–Nordeng also produces highly intermittent precipitation, with a very quick decrease in the precipitation temporal autocorrelation (this is also the case in the global ECHAM–HAM setup, not shown). CCFM gives results in much better agreement with the 10-min radar observations. This is a major improvement compared to Tiedtke–Nordeng, and we believe it is related to a better treatment of the triggering, based on the use of a subcloud entraining plume model and hence directly linked to boundary layer temperature and moisture profiles. Decreasing the entrainment decreases the impact of environmental air temperature and humidity on the rising parcel and appears to slightly increase the intermittency of precipitation (Fig. 6b). However, this is only a small change, and CCFM remains much closer to the radar observations than Tiedtke–Nordeng.

The precipitation intensity distribution (Fig. 6c) cannot be estimated with the Tiedtke–Nordeng scheme as there is no explicit calculation of the convective column area. We assume that each cloud in CCFM has horizontally homogeneous precipitation falling under the cloud maximum horizontal area. We then calculate the precipitation-weighted probability distribution of below-cloud precipitation rates for the CCFM convective clouds, as well as for the CPOL-observed clouds:

$$P_i = \frac{\sum_{i<R\le i+1} R \times (R \times \text{area})}{\sum (R \times \text{area})}, \tag{4}$$

with R the below-cloud precipitation rate (average precipitation rate over 2.5 km × 2.5 km for the radar data) and i an integer between 0 and 300 mm h^{-1} (only 0–150 mm h^{-1} is shown; Fig. 6c). Hence, "precipitation weighting" means here that the area under the curve in a given interval of precipitation rate is the fraction of the total precipitation in this interval (the area over all the precipitation bins is normalized).

The radar-observed total precipitation distribution is close to an exponential distribution for precipitation

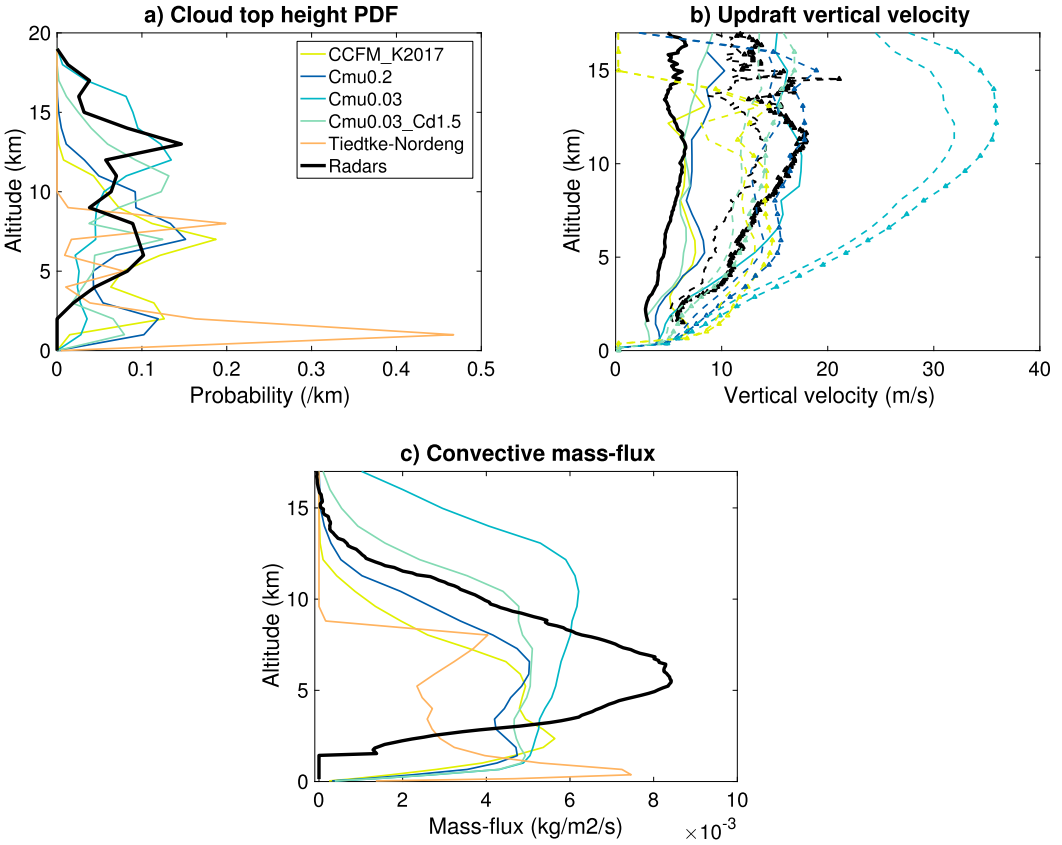

FIG. 5. As in Figs. 3 and 4, but for selected parameter configurations only to summarize and illustrate the impact of low entrainment and low entrainment–high drag configurations.

larger than 10 mm h^{-1} (Fig. 6c). The probability density reaches a maximum for precipitation rates between 1 and 2 mm h^{-1}. The observed distribution of convective precipitation rate is very different from the distribution of total precipitation (convective and stratiform) and has a clear maximum at 17 mm h^{-1}.

All CCFM configurations as well as the Tiedtke–Nordeng scheme largely overestimate the proportion of convective precipitation (about 95% for CCFM and 76% and 98%, respectively, for the base Tiedtke–Nordeng simulation and the one with low entrainment) compared to the radar observations (42%). With CCFM, the intense stratiform precipitation is not represented at all (there is no stratiform precipitation rate above 2 mm h^{-1}), and hence, the stratiform precipitation makes only a limited contribution to the simulated distribution of total precipitation. This strong underestimation of stratiform precipitation has also been observed with cloud-resolving models and limited-area models (Varble et al. 2014b) and in their case traced back to deficiencies in the microphysics. In CCFM, a too-large fraction of the total precipitation comes from intense below-cloud precipitation rates (Fig. 6c), as also observed with a higher-resolution model using a mass flux parameterization (Nguyen et al. 2015).

We also note that decreasing the entrainment parameter leads to more frequent large precipitation rates and less precipitation at very low rates. Other studies using bulk mass flux parameterization have shown similar sensitivity of precipitation-rate distribution when the entrainment rate is changed (Bush et al. 2015). This is partly counterbalanced by adding drag (C_d = 1.5), which tends to reduce the intensity of convection.

Deficiencies of all CCFM configurations in representing the distribution of below-cloud precipitation rates are mostly due to too-few, too-narrow updrafts: the total convective area fraction is too small (leading to too-large below-cloud precipitation rates; cf. Fig. 6c), largely because weak updrafts are missing in CCFM, while they account for a significant convective area fraction in the observations (cf. Fig. S7 and section S3). This is likely due to an intrinsic limitation of CCFM as each CCFM cloud type has only one mean vertical

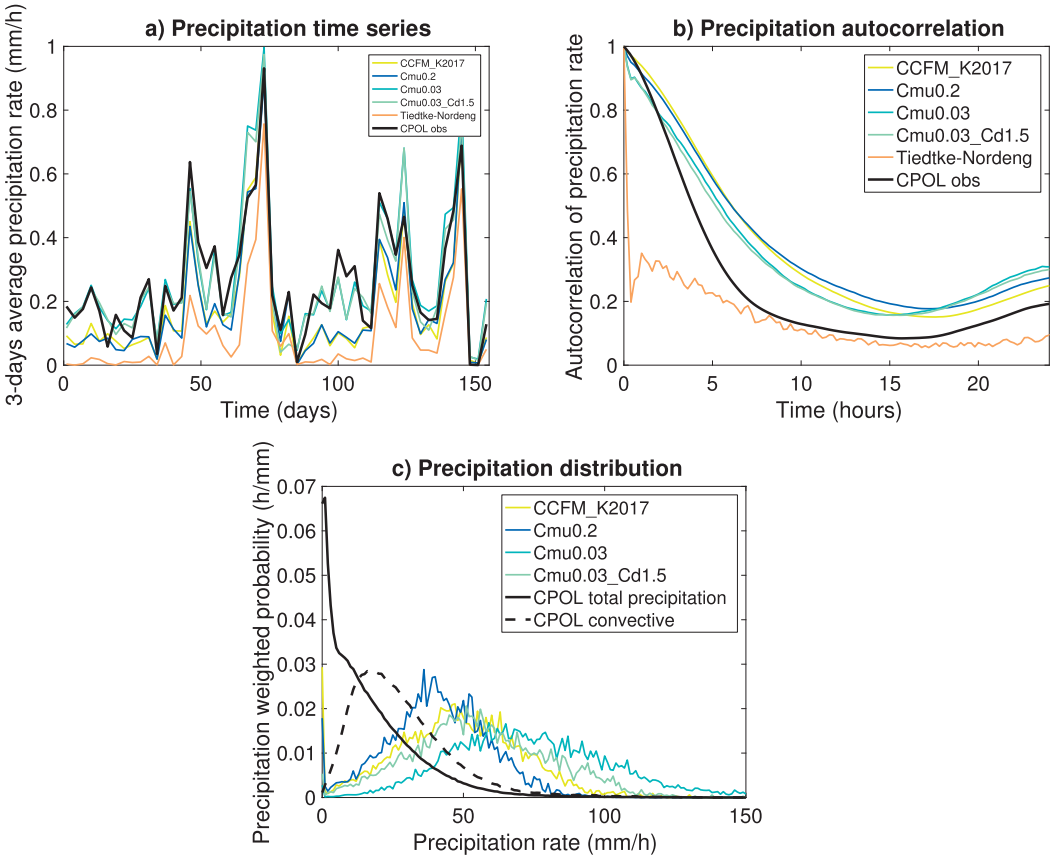

FIG. 6. Precipitation at Darwin from CPOL 10-min retrievals and from the SCM with different convective parameterizations. (a) Average total precipitation rates from the 10-min CPOL observations (black) and from the 12-min SCM simulations with the Tiedtke–Nordeng bulk mass flux scheme (orange line, when available) and different configurations of CCFM (cf. Table 1). (b) Time autocorrelation of the total precipitation rates. (c) Precipitation-weighted probability distribution of below-cloud convective precipitation rates (bins of 1 mm h^{-1}). The dashed line is obtained by considering only convective precipitation.

velocity and is described by a simple plume model. Further CCFM improvement could include a representation of shear and a more detailed representation of convective updrafts (and possibly downdrafts) and of entrainment, but this will need significant additional model development and is beyond the scope of the present study.

5. Conclusions and perspectives

We compared single-column simulations of ECHAM6.1–HAM2.2 using two different convective parameterizations during the wet season at Darwin, Australia, with radar retrievals of convective cloud properties: vertical velocities, cloud-top-height distribution, precipitation rates, and mass fluxes. These radar data allow for an in-depth analysis of model performances: we showed how long-term radar measurements (using three radars operating at different wavelengths) open new pathways for evaluation of internal parameterization variables and inform further parameterization development.

The spectral convective parameterization convective cloud field model (CCFM) produces better results than the bulk mass flux Tiedtke–Nordeng scheme in representing the cloud-top-height distributions and the precipitation rates, avoiding the unrealistic high-frequency intermittency of precipitation produced by the Tiedtke–Nordeng scheme. To a lesser extent, mass flux profiles are also improved.

We showed the importance of the entrainment parameter for driving the CCFM-simulated cloud spectrum. A low entrainment parameter is needed in order to have a large-enough buoyancy and to produce enough deep convective clouds, which is essential to accurately capture the radiative effect of convective clouds. However, a low entrainment parameter also leads to a substantial overestimation of the vertical velocity (when compared to the radar retrievals). This has strong limitations for aerosol–cloud interactions as an accurate

updraft velocity is needed to estimate the right number of activated aerosol (West et al. 2014; Sullivan et al. 2016), for the microphysics, and hence possibly for climate forcing (Donner et al. 2016). To reduce the vertical velocity without reducing the buoyancy, we increased the poorly constrained aerodynamic drag parameter (originally set to zero) in the rising plume equation of motion. This gives good results in terms of both the cloud-top-height distribution and the mean and high percentiles of vertical velocity profiles. This configuration represents the observed time series and temporal variability of precipitation rates well but overestimates (as all CCFM configurations) the below-cloud precipitation rates, primarily because of too-narrow convective plumes.

Hence, the spectral convection parameterization CCFM can represent the main features of the convective cloud spectrum in the tropical western Pacific, although some differences remain in the mass flux profiles, the details of the cloud-top-height distributions, and the distribution of vertical velocity. CCFM is designed to represent shallow and deep convective updrafts but cannot reproduce the weakest updrafts observed and hence tends to produce too-strong, too-narrow updrafts. Even high-resolution models have difficulties reproducing the characteristics of convective updrafts in this region and, as in our simulations, often overestimate vertical velocities (e.g., Varble et al. 2014a). The remaining differences between CCFM and the observations are likely to be linked to intrinsic assumptions made in CCFM: real clouds differ from rising plumes with a simple formulation of entrainment and drag and one mean vertical velocity per cloud, and the atmosphere is not in quasi equilibrium at short time scales. Comparing CCFM with LES models of convective clouds could help further improve the plume model, but we believe a new formulation is needed to produce significant improvements. Although some further investigations and development are always needed in a convective parameterization, the present study suggests that ECHAM–HAM–CCFM meets some of the basic requirements for representing a population of convective clouds, at least in the TWP-ICE area.

The 2D radar retrievals have been essential in this study and should provide important constraints for evaluation and development of future convective parameterizations. However, further investigations of CCFM (and other parameterizations) could be conducted by using a new 3D dataset of convective vertical velocity in the Darwin area currently under development. This would allow for a more direct calculation of the convective mass flux and hence be less subject to representativity issues. Such a dataset could also allow more relevant stratification by water vapor content, which is known to be an important variable for convective growth (Holloway and Neelin 2010; Labbouz et al. 2015) but seems to have too little impact on CCFM, as in most current models (Del Genio 2012). Further stratification should be considered in future studies to gain better understanding of model performances and possibilities for improvements. We will also consider using radar datasets at other locations when they are available along with good-quality meteorological data and analysis products to drive the SCM. Comparison of these extended datasets with an ensemble of model simulations would make it possible to evaluate not only CCFM itself but also the impacts and feedbacks of CCFM on the large scale and hence provide a new framework for continuous development, possibly including more fundamental changes in the model (for instance, departure from quasi equilibrium and development of a new plume model).

Acknowledgments. The research leading to these results has received funding from the European Union's Seventh Framework Programme (FP7/2007-2013) Project BACCHUS under Grant Agreement 603445 and the European Research Council under the European Union's Seventh Framework Programme (FP7/2007–2013)/ERC Grant Agreement FP7–280025 (ACCLAIM) and under the European Union's Horizon 2020 research and innovation program with Grant Agreement 724602 (RECAP). The ECHAM–HAMMOZ model is developed by a consortium composed of ETH Zürich, Max Planck Intitut für Meteorologie, Forschungzentrum Jülich, the University of Oxford, and the Finnish Meteorological Institute and managed by the Center for Climate Systems Modeling (C2SM) at ETH Zürich.

We thank the three anonymous reviewers for their questions and comments that helped to improve the manuscript.

The data used to drive and relax the SCM simulations have been produced by the Department of Energy (DOE) Atmospheric Radiation Measurement (ARM) Program under Grants DE-FG02-03ER63533 and DE-FG02-08ER64527. They can be accessed via the ARM website (https://doi.org/10.5439/1171946). Model simulation outputs can be obtained by contacting the corresponding author. The model source code can be accessed via the HAMMOZ SVN repository (https://svn.iac.ethz.ch/external/echam-hammoz/echam6-hammoz/branches/uni_oxford_climate_processes/CCFM_P3_2.4.7) under the revision number 4030 (cf. the HAMMOZ Redmine for access and licensing conditions: https://redmine.hammoz.ethz.ch/projects/hammoz/wiki).

REFERENCES

Abdul-Razzak, H., and S. J. Ghan, 2000: A parameterization of aerosol activation: 2. Multiple aerosol types. *J. Geophys. Res.*, **105**, 6837–6844, https://doi.org/10.1029/1999JD901161.

Arakawa, A., and W. H. Schubert, 1974: Interaction of a cumulus cloud ensemble with the large-scale environment, part I. *J. Atmos. Sci.*, **31**, 674–701, https://doi.org/10.1175/1520-0469(1974)031<0674:IOACCE>2.0.CO;2.

Bechtold, P., E. Bazile, F. Guichard, P. Mascart, and E. Richard, 2001: A mass-flux convection scheme for regional and global models. *Quart. J. Roy. Meteor. Soc.*, **127**, 869–886, https://doi.org/10.1002/qj.49712757309.

Brennen, C. E., 1982: A review of added mass and fluid inertial forces. Naval Civil Engineering Laboratory Rep. CR 82.010, 55 pp., http://resolver.caltech.edu/CaltechAUTHORS:BREncel82.

Bretherton, C. S., J. R. McCaa, and H. Grenier, 2004: A new parameterization for shallow cumulus convection and its application to marine subtropical cloud-topped boundary layers. Part I: Description and 1D results. *Mon. Wea. Rev.*, **132**, 864–882, https://doi.org/10.1175/1520-0493(2004)132<0864:ANPFSC>2.0.CO;2.

Bush, S. J., A. G. Turner, S. J. Woolnough, G. M. Martin, and N. P. Klingaman, 2015: The effect of increased convective entrainment on Asian monsoon biases in the MetUM general circulation model. *Quart. J. Roy. Meteor. Soc.*, **141**, 311–326, https://doi.org/10.1002/qj.2371.

Dawe, J. T., and P. H. Austin, 2013: Direct entrainment and detrainment rate distributions of individual shallow cumulus clouds in an LES. *Atmos. Chem. Phys.*, **13**, 7795–7811, https://doi.org/10.5194/acp-13-7795-2013.

Del Genio, A. D., 2012: Representing the sensitivity of convective cloud systems to tropospheric humidity in general circulation models. *Surv. Geophys.*, **33**, 637–656, https://doi.org/10.1007/s10712-011-9148-9.

Derbyshire, S. H., I. Beau, P. Bechtold, J.-Y. Grandpeix, J.-M. Piriou, J.-L. Redelsperger, and P. M. M. Soares, 2004: Sensitivity of moist convection to environmental humidity. *Quart. J. Roy. Meteor. Soc.*, **130**, 3055–3079, https://doi.org/10.1256/qj.03.130.

Donner, L. J., T. A. O'Brien, D. Rieger, B. Vogel, and W. F. Cooke, 2016: Are atmospheric updrafts a key to unlocking climate forcing and sensitivity? *Atmos. Chem. Phys.*, **16**, 12 983–12 992, https://doi.org/10.5194/acp-16-12983-2016.

Franklin, C. N., C. Jakob, M. Dix, A. Protat, and G. Roff, 2012: Assessing the performance of a prognostic and a diagnostic cloud scheme using single column model simulations of TWP–ICE. *Quart. J. Roy. Meteor. Soc.*, **138**, 734–754, https://doi.org/10.1002/qj.954.

Ghan, S., and Coauthors, 2000: A comparison of single column model simulations of summertime midlatitude continental convection. *J. Geophys. Res.*, **105**, 2091–2124, https://doi.org/10.1029/1999JD900971.

Gregory, D., 2001: Estimation of entrainment rate in simple models of convective clouds. *Quart. J. Roy. Meteor. Soc.*, **127**, 53–72, https://doi.org/10.1002/qj.49712757104.

Guérémy, J. F., 2011: A continuous buoyancy based convection scheme: One- and three-dimensional validation. *Tellus*, **63A**, 687–706, https://doi.org/10.1111/j.1600-0870.2011.00521.x.

Holloway, C. E., and J. D. Neelin, 2010: Temporal relations of column water vapor and tropical precipitation. *J. Atmos. Sci.*, **67**, 1091–1105, https://doi.org/10.1175/2009JAS3284.1.

Kain, J. S., and J. M. Fritsch, 1990: A one-dimensional entraining/detraining plume model and its application in convective parameterization. *J. Atmos. Sci.*, **47**, 2784–2802, https://doi.org/10.1175/1520-0469(1990)047<2784:AODEPM>2.0.CO;2.

Kim, D., and I.-S. Kang, 2012: A bulk mass flux convection scheme for climate model: Description and moisture sensitivity. *Climate Dyn.*, **38**, 411–429, https://doi.org/10.1007/s00382-010-0972-2.

Kipling, Z., P. Stier, L. Labbouz, and T. Wagner, 2017: Dynamic subgrid heterogeneity of convective cloud in a global model: Description and evaluation of the convective cloud field model (CCFM) in ECHAM6–HAM2. *Atmos. Chem. Phys.*, **17**, 327–342, https://doi.org/10.5194/acp-17-327-2017.

Kumar, V. V., C. Jakob, A. Protat, C. R. Williams, and P. T. May, 2015: Mass-flux characteristics of tropical cumulus clouds from wind profiler observations at Darwin, Australia. *J. Atmos. Sci.*, **72**, 1837–1855, https://doi.org/10.1175/JAS-D-14-0259.1.

Labbouz, L., J. Van Baelen, and C. Duroure, 2015: Investigation of the links between water vapor field evolution and rain rate based on five years of measurements at a midlatitude site. *Geophys. Res. Lett.*, **42**, 9538–9545, https://doi.org/10.1002/2015GL066048.

Levine, J., 1959: Spherical vortex theory of bubble-like motion in cumulus clouds. *J. Meteor.*, **16**, 653–662, https://doi.org/10.1175/1520-0469(1959)016<0653:SVTOBL>2.0.CO;2.

Lohmann, U., and C. Hoose, 2009: Sensitivity studies of different aerosol indirect effects in mixed-phase clouds. *Atmos. Chem. Phys.*, **9**, 8917–8934, https://doi.org/10.5194/acp-9-8917-2009.

——, P. Stier, C. Hoose, S. Ferrachat, S. Kloster, E. Roeckner, and J. Zhang, 2007: Cloud microphysics and aerosol indirect effects in the global climate model ECHAM5-HAM. *Atmos. Chem. Phys.*, **7**, 3425–3446, https://doi.org/10.5194/acp-7-3425-2007.

May, P. T., J. H. Mather, G. Vaughan, K. N. Bower, C. Jakob, G. M. McFarquhar, and G. G. Mace, 2008: The Tropical Warm Pool International Cloud Experiment. *Bull. Amer. Meteor. Soc.*, **89**, 629–645, https://doi.org/10.1175/BAMS-89-5-629.

Möbis, B., and B. Stevens, 2012: Factors controlling the position of the intertropical convergence zone on an aquaplanet. *J. Adv. Model. Earth Syst.*, **4**, M00A04, https://doi.org/10.1029/2012MS000199.

Moorthi, S., and M. J. Suarez, 1992: Relaxed Arakawa–Schubert. A parameterization of moist convection for general circulation models. *Mon. Wea. Rev.*, **120**, 978–1002, https://doi.org/10.1175/1520-0493(1992)120<0978:RASAPO>2.0.CO;2.

Neggers, R. J., A. P. Siebesma, and T. Heus, 2012: Continuous single-column model evaluation at a permanent meteorological supersite. *Bull. Amer. Meteor. Soc.*, **93**, 1389–1400, https://doi.org/10.1175/BAMS-D-11-00162.1.

Nguyen, H., A. Protat, V. Kumar, S. Rauniyar, M. Whimpey, and L. Rikus, 2015: A regional forecast model evaluation of statistical rainfall properties using the CPOL radar observations in different precipitation regimes over Darwin, Australia. *Quart. J. Roy. Meteor. Soc.*, **141**, 2337–2349, https://doi.org/10.1002/qj.2525.

Nober, F. J., and H. F. Graf, 2005: A new convective cloud field model based on principles of self-organisation. *Atmos. Chem. Phys.*, **5**, 2749–2759, https://doi.org/10.5194/acp-5-2749-2005.

Nordeng, T. E., 1994: Extended versions of the convection parametrization scheme at ECMWF and their impact upon the mean climate and transient activity of the model in the tropics. ECMWF Tech. Memo. 206, 41 pp., https://www.ecmwf.int/sites/default/files/elibrary/1994/11393-extended-versions-convective-parametrization-scheme-ecmwf-and-their-impact-mean-and-transient.pdf.

Pantaleone, J., and J. Messer, 2011: The added mass of a spherical projectile. *Amer. J. Phys.*, **79**, 1202–1210, https://doi.org/10.1119/1.3644334.

Petch, J., A. Hill, L. Davies, A. Fridlind, C. Jakob, Y. Lin, S. Xie, and P. Zhu, 2014: Evaluation of intercomparisons of four different types of model simulating TWP-ICE. *Quart. J. Roy. Meteor. Soc.*, **140**, 826–837, https://doi.org/10.1002/qj.2192.

Plant, R. S., and G. C. Craig, 2008: A stochastic parameterization for deep convection based on equilibrium statistics. *J. Atmos. Sci.*, **65**, 87–105, https://doi.org/10.1175/2007JAS2263.1.

Protat, A., and C. R. Williams, 2011: The accuracy of radar estimates of ice terminal fall speed from vertically pointing Doppler radar measurements. *J. Appl. Meteor. Climatol.*, **50**, 2120–2138, https://doi.org/10.1175/JAMC-D-10-05031.1.

Pruppacher, H. R., and J. D. Klett, 1997: *Microphysics of Clouds and Precipitation.* Springer, 975 pp.

Randall, D. A., K. Xu, R. J. C. Somerville, and S. Iacobellis, 1996: Single-column models and cloud ensemble models as links between observations and climate models. *J. Climate*, **9**, 1683–1697, https://doi.org/10.1175/1520-0442(1996)009<1683:SCMACE>2.0.CO;2.

Romps, D. M., and A. B. Charn, 2015: Sticky thermals: Evidence for a dominant balance between buoyancy and drag in cloud updrafts. *J. Atmos. Sci.*, **72**, 2890–2901, https://doi.org/10.1175/JAS-D-15-0042.1.

Saunders, P. M., 1962: Penetrative convection in stably stratified fluids. *Tellus*, **14**, 177–194, https://doi.org/10.3402/tellusa.v14i2.9539.

Sherwood, S. C., D. Hernández-Deckers, M. Colin, and F. Robinson, 2013: Slippery thermals and the cumulus entrainment paradox. *J. Atmos. Sci.*, **70**, 2426–2442, https://doi.org/10.1175/JAS-D-12-0220.1.

Simpson, J., and V. Wiggert, 1969: Models of precipitating cumulus towers. *Mon. Wea. Rev.*, **97**, 471–489, https://doi.org/10.1175/1520-0493(1969)097<0471:MOPCT>2.3.CO;2.

——, R. H. Simpson, D. A. Andrews, and M. A. Eaton, 1965: Experimental cumulus dynamics. *Rev. Geophys.*, **3**, 387–431, https://doi.org/10.1029/RG003i003p00387.

Song, H., W. Lin, Y. Lin, A. B. Wolf, R. Neggers, L. J. Donner, A. D. Del Genio, and Y. Liu, 2013: Evaluation of precipitation simulated by seven SCMs against the ARM observations at the SGP site. *J. Climate*, **26**, 5467–5492, https://doi.org/10.1175/JCLI-D-12-00263.1.

Stevens, B., and Coauthors, 2013: Atmospheric component of the MPI-M Earth System Model: ECHAM6. *J. Adv. Model. Earth Syst.*, **5**, 146–172, https://doi.org/10.1002/jame.20015.

Stier, P., and Coauthors, 2005: The aerosol-climate model ECHAM5-HAM. *Atmos. Chem. Phys.*, **5**, 1125–1156, https://doi.org/10.5194/acp-5-1125-2005.

Sullivan, S. C., D. Lee, L. Oreopoulos, and A. Nenes, 2016: Role of updraft velocity in temporal variability of global cloud hydrometeor number. *Proc. Natl. Acad. Sci. USA*, **113**, 5791–5796, https://doi.org/10.1073/pnas.1514039113.

Thurai, M., V. N. Bringi, and P. T. May, 2010: CPOL radar-derived drop size distribution statistics of stratiform and convective rain for two regimes in Darwin, Australia. *J. Atmos. Oceanic Technol.*, **27**, 932–942, https://doi.org/10.1175/2010JTECHA1349.1.

Tiedtke, M., 1989: A comprehensive mass flux scheme for cumulus parameterization in large-scale models. *Mon. Wea. Rev.*, **117**, 1779–1800, https://doi.org/10.1175/1520-0493(1989)117<1779:ACMFSF>2.0.CO;2.

Turner, J. S., 1963: The motion of buoyant elements in turbulent surroundings. *J. Fluid Mech.*, **16**, 1–16, https://doi.org/10.1017/S0022112063000549.

Varble, A., and Coauthors, 2014a: Evaluation of cloud-resolving and limited area model intercomparison simulations using TWP-ICE observations: 1. Deep convective updraft properties. *J. Geophys. Res. Atmos.*, **119**, 13 891–13 918, https://doi.org/10.1002/2013JD021371.

——, and Coauthors, 2014b: Evaluation of cloud-resolving and limited area model intercomparison simulations using TWP-ICE observations: 2. Precipitation microphysics. *J. Geophys. Res. Atmos.*, **119**, 13 919–13 945, https://doi.org/10.1002/2013JD021372.

Wagner, T. M., and H.-F. Graf, 2010: An ensemble cumulus convection parameterization with explicit cloud treatment. *J. Atmos. Sci.*, **67**, 3854–3869, https://doi.org/10.1175/2010JAS3485.1.

Wang, X., and M. Zhang, 2014: Vertical velocity in shallow convection for different plume types. *J. Adv. Model. Earth Syst.*, **6**, 478–489, https://doi.org/10.1002/2014MS000318.

West, R. E. L., P. Stier, A. Jones, C. E. Johnson, G. W. Mann, N. Bellouin, D. G. Partridge, and Z. Kipling, 2014: The importance of vertical velocity variability for estimates of the indirect aerosol effects. *Atmos. Chem. Phys.*, **14**, 6369–6393, https://doi.org/10.5194/acp-14-6369-2014.

Williams, C. R., 2012: Vertical air motion retrieved from dual-frequency profiler observations. *J. Atmos. Oceanic Technol.*, **29**, 1471–1480, https://doi.org/10.1175/JTECH-D-11-00176.1.

Xie, S., R. T. Cederwall, and M. Zhang, 2004: Developing long-term single-column model/cloud system–resolving model forcing data using numerical weather prediction products constrained by surface and top of the atmosphere observations. *J. Geophys. Res.*, **109**, D01104, https://doi.org/10.1029/2003JD004045.

——, T. Hume, C. Jakob, S. A. Klein, R. B. McCoy, and M. Zhang, 2010: Observed large-scale structures and diabatic heating and drying profiles during TWP-ICE. *J. Climate*, **23**, 57–79, https://doi.org/10.1175/2009JCLI3071.1.

Yoshimura, H., R. Mizuta, and H. Murakami, 2015: A spectral cumulus parameterization scheme interpolating between two convective updrafts with semi-Lagrangian calculation of transport by compensatory subsidence. *Mon. Wea. Rev.*, **143**, 597–621, https://doi.org/10.1175/MWR-D-14-00068.1.

Zhang, J., U. Lohmann, and P. Stier, 2005: A microphysical parameterization for convective clouds in the ECHAM5 climate model: Single-column model results evaluated at the Oklahoma Atmospheric Radiation Measurement Program site. *J. Geophys. Res.*, **110**, D15S07, https://doi.org/10.1029/2004JD005128.

Zhang, K., and Coauthors, 2012: The global aerosol-climate model ECHAM-HAM, version 2: Sensitivity to improvements in process representations. *Atmos. Chem. Phys.*, **12**, 8911–8949, https://doi.org/10.5194/acp-12-8911-2012.

Zhang, M. H., and J. L. Lin, 1997: Constrained variational analysis of sounding data based on column-integrated budgets of mass, heat, moisture, and momentum: Approach and application to ARM measurements. *J. Atmos. Sci.*, **54**, 1503–1524, https://doi.org/10.1175/1520-0469(1997)054<1503:CVAOSD>2.0.CO;2.

——, and Coauthors, 2013: CGILS: Results from the first phase of an international project to understand the physical mechanisms of low cloud feedbacks in single column models. *J. Adv. Model. Earth Syst.*, **5**, 826–842, https://doi.org/10.1002/2013MS000246.

——, R. C. J. Somerville, and S. Xie, 2016: The SCM concept and creation of ARM forcing datasets. *The Atmospheric Radiation Measurement (ARM) Program: The First 20 Years*, *Meteor. Monogr.*, No. 57, Amer. Meteor. Soc., https://doi.org/10.1175/AMSMONOGRAPHS-D-15-0040.1.